Cell Reports
Methods

Article

Engineering protein activity into off-the-shelf DNA devices

Graphical abstract

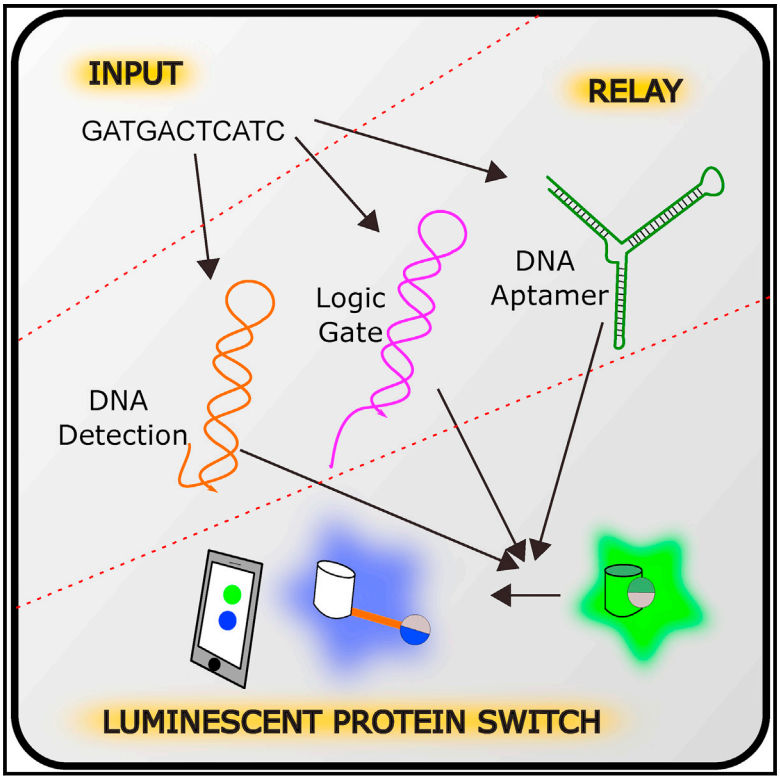

Authors

Harsimranjit Sekhon, Stewart N. Loh

Correspondence

lohs@upstate.edu

In brief

Sekhon and Loh develop a luminescent protein switch that undergoes a conformational change in response to various DNA inputs, switching its color from green to blue. This protein is paired with DNA engineering techniques to detect specific DNA sequences and small molecules and process two-input logic gates.

Highlights

- nLuc-AFF is a luminescent protein switch whose color is controlled by DNA inputs
- nLuc-AFF is functional in serum, and its output is quantified by phone camera
- Sensor output is controlled by DNA sequences, logic gates, and aptamers
- Technique can potentially convert other proteins to DNA/RNA-activated switches

Sekhon & Loh, 2022, Cell Reports Methods 2, 100202
April 25, 2022
https://doi.org/10.1016/j.crmeth.2022.100202

CellPress

Cell Reports Methods

CellPress
OPEN ACCESS

Article

Engineering protein activity into off-the-shelf DNA devices

Harsimranjit Sekhon[1] and Stewart N. Loh[1,2,*]
[1]Department of Biochemistry and Molecular Biology, SUNY Upstate Medical University, Syracuse, NY 13210, USA
[2]Lead contact
*Correspondence: lohs@upstate.edu
https://doi.org/10.1016/j.crmeth.2022.100202

MOTIVATION Nature has given us an example of proteins, the Cas enzymes, that are activated by binding specific DNA or RNA sequences. Cas enzymes possess the lone function of cleaving nucleic acids, yet they have given rise to a gene-editing technology that has transformed biology. It has not yet been feasible to introduce this mode of control into other proteins and enzymes. Here, we fuse a DNA-binding domain (GCN4) to an enzyme (nanoluciferase) such that binding a specific DNA sequence to the former triggers a conformational change in the latter, resulting in a ratiometric green-to-blue luminescence change. This protein switch plugs into existing DNA tools to generate a biosensor for DNA and RNA sequences of choice, as well as for small molecules and proteins. This mechanism is general—based on established principles of protein folding and nucleic acid base pairing—and has the potential to access the biological activity of the proteome to regulation by nucleic acids and other biomolecules.

SUMMARY

DNA-based devices are straightforward to design by virtue of their predictable folding, but they lack complex biological activity such as catalysis. Conversely, protein-based devices offer a myriad of functions but are much more difficult to design due to their complex folding. This study combines DNA and protein engineering to generate an enzyme that is activated by a DNA sequence of choice. A single protein switch, engineered from nanoluciferase using the alternate-frame-folding mechanism and herein called nLuc-AFF, is paired with different DNA technologies to create a biosensor for specific nucleic acid sequences, sensors for serotonin and ATP, and a two-input logic gate. nLuc-AFF is a genetically encoded, ratiometric, blue/green-luminescent biosensor whose output can be quantified by a phone camera. nLuc-AFF retains ratiometric readout in 100% serum, making it suitable for analyzing crude samples in low-resource settings. This approach can be applied to other proteins and enzymes to convert them into DNA-activated switches.

INTRODUCTION

Structural biology of proteins and nucleic acids has given rise to a diverse set of methods for biomolecular engineering. DNA building blocks have been used to create self-assembling nanostructures (Ong et al., 2017; Whitesides and Grzybowski, 2002; Woods et al., 2019; Yin et al., 2008), tools for the detection of other biomolecules (Bracaglia et al., 2021; Chandrasekaran and Halvorsen, 2021; Choi et al., 2014, 2018; Krishnan et al., 2020; Saka et al., 2019), and ribocomputing devices that control gene expression based on various inputs (Green et al., 2017; Kim et al., 2018). *De novo* protein design and modifications of existing proteins have also spawned a toolbox of biotechnologies for use in molecular detection (Quijano-Rubio et al., 2021; Stratton et al., 2008; Zheng et al., 2014), allosteric (Karchin et al., 2017; Langan et al., 2019) and optogenetic (Stone et al., 2019) control of biological activity, and many more applications. The simple phosphodiester backbone/nucleoside base architecture, the linear and binary nature of base-pairing interactions, and the facile nature of DNA/RNA synthesis combine to make creating nucleic acid structures with desired structures and properties relatively straightforward. Their structural and chemical simplicity, however, render nucleic acids (except for certain RNAs) devoid of complex biological functions such as catalysis. To compensate for this, fluorescent dyes, photoreactive compounds, peptides, and other groups can be chemically attached to integrate biological activity into DNA tools (Madsen and Gothelf, 2019).

In contrast to DNA, proteins catalyze innumerable reactions and perform all the intricate functions required for life. However, proteins are much more difficult to design *de novo*, and modifying natural proteins often produces unpredictable results.

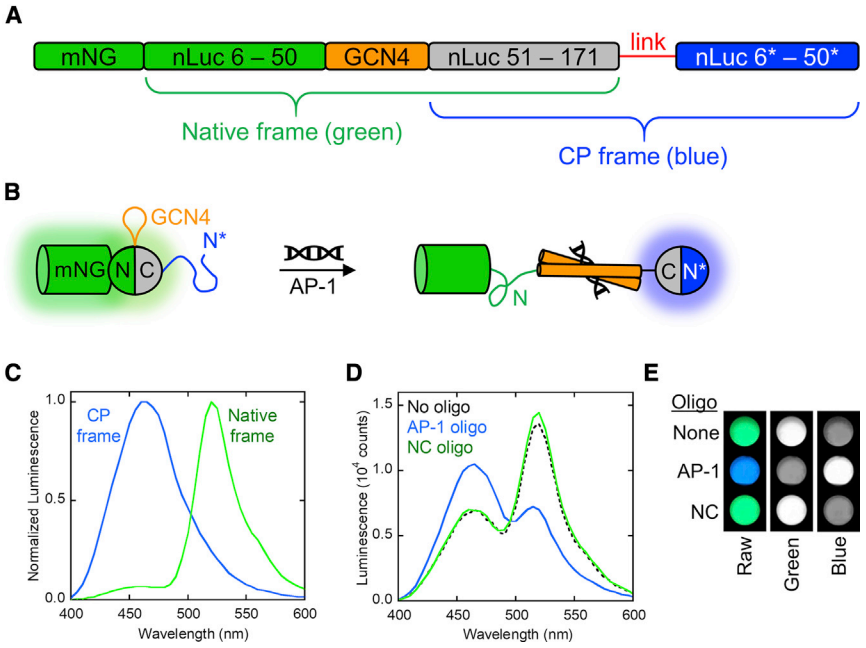

Figure 1. Design and characterization of the nLuc-AFF switch

(A) The GCN4 binding domain (orange) was inserted between residues 50–51 of the nLuc domain of the GeNL protein (green and gray) to create the native frame of the switch (green-orange-gray). To establish the CP frame of the switch (gray-red-blue), the segment of nLuc that was N-terminal to GCN4 (residues 6–50) was then duplicated (residues 6*–50*; blue) and appended to the C terminus using a 6-aa linker (red). nLuc-AFF can fold either in the native frame (green luminescence) or the CP frame (blue luminescence) but not both.

(B) The green-to-blue luminescence change is triggered by DNA-binding-induced folding of the GCN4 domain, which stretches and unfolds the native frame and forces nLuc-AFF to fold in the CP frame. This fold shift separates the mNG a nd nLuc domains and causes luminescence to change from green to blue. Only one monomer of the GCN4 dimer is shown for clarity.

(C) The isolated native and CP frames exhibited the expected green and blue luminescence spectra, respectively.

(D) nLuc-AFF emitted mostly green light in the absence of DNA as well as in the presence of nonconsensus (NC) DNA and emitted mostly blue light in the presence of AP-1 DNA.

(E) The green-to-blue color change upon AP-1 binding was visible in raw cell-phone pictures as well as by isolating individual green and blue channels from phone images.

Sensor concentration was 30 nM in (D) and (E).

The fields of nucleic acid and protein engineering have largely evolved independently, with little overlap between the two. In this study, we combine these approaches to give rise to a class of protein switches whose enzymatic function can be activated by a DNA input. We use well-developed DNA engineering techniques to activate a color-changing ratiometric luminescent biosensor constructed using the alternate frame folding (AFF) mechanism.

AFF is a protein engineering approach that introduces allostery into a protein that has none (Stratton et al., 2008). The target protein is constructed such that it can adopt either its native fold or one corresponding to a circular permutant (CP). The ability to fold into one of two "frames" in a mutually exclusive fashion is enabled by duplicating an N-terminal (or C-terminal) segment of the protein and fusing it to the opposite end of the wild-type (WT) protein using a linker peptide long enough to span the distance between the protein's original N- and C termini (Figure 1A). The central, shared segment can then fold with either of the duplicated segments but not both. Different functions can be assigned to each fold by introducing mutations or fusing proteins to either duplicate segment. Examples of different functions include the presence and absence of enzymatic/binding activity or changing the color of emitted light, the latter of which we do here.

Linking the fold shift to ligand binding is achieved by inserting a disordered binding domain into one of the frames. Provided that the binding domain folds upon encountering the ligand and has a reasonably long (>20 Å) N-to-C-terminal distance when folded, this reaction stretches the structure of the fold in which it resides, causing the target protein to switch to the other folding frame.

Our goal was to apply this methodology to make a generalizable luminescent biosensor that changes from green to blue emission upon activation of a DNA-based device. This allows the use of the same biosensor to sense a variety of ligands by using DNA devices to relay ligand binding to allosteric control of protein activity. We chose to base the AFF scaffold on nanoluciferase (nLuc; a blue luminescent protein derived from deep-sea shrimp *Oplophorus gracilirostris*) because it possesses high thermodynamic stability (Hall et al., 2012) (which helps it retain function after domain insertion and circular permutation), is the brightest luciferase currently known (England et al., 2016), and has been split, permuted, and fused in a number of biosensor designs (Biewenga et al., 2020; Guo et al., 2022). To establish the blue and green states of the sensor, we employed the variant of nLuc (green enhanced nanolantern [GeNL]) in which the GFP variant mNeonGreen (mNG) was fused to the N terminus of nLuc (Suzuki et al., 2016). The blue emission of nLuc is captured by mNG and is essentially completely converted to green fluorescence via bioluminescence resonance energy transfer (BRET). For efficient resonant coupling, it was essential to bring the two proteins into proximity by deleting the first four amino acids of nLuc and the last ten amino acids of mNG (Suzuki et al., 2016).

Our hypothesis was that a green/blue luminescent switch could be engineered by introducing an intramolecular conformational change that extinguishes luminescence of the nLuc domain fused to mNG and turns on luminescence of a second, circularly permuted nLuc within the same molecule via the AFF mechanism. As a result of the AFF conformational change, permuted nLuc becomes separated from mNG by a >100

amino-acid segment, the length of which is predicted to be >75 Å (*vide infra*). Permuted nLuc is thus expected to emit blue luminescence (Figure 1B). To couple this conformational change to DNA binding, we turned to the GCN4 DNA-binding domain as the input domain. GCN4 is a 56 amino-acid peptide consisting of a constitutively dimerized, C-terminal leucine zipper and an N-terminal DNA-binding region that is largely unstructured in the absence of its 11-nucleotide consensus DNA sequence (AP-1). GCN4 folds into a rigid, rod-shaped molecule of 75 Å in length when bound to AP-1 (O'Shea et al., 1991) (Figure 1B). We previously applied this folding reaction to stretch and unfold the enzyme barnase in the GCN4-barnase fusion protein (Ha et al., 2006). We incorporate the AP-1 sequence into off-the-shelf DNA devices to construct two-input logic gates as well as biosensors for ATP and serotonin.

Existing DNA-based devices can perform many of the sensing functions described herein without a protein component. The protein component obviates the need to chemically derivatize the DNA tools and provides the additional benefits of bioluminescent output and genetic encoding. The main impact of this study, however, is that the AFF methodology can be applied to other proteins and enzymes to convert them into DNA- and RNA-activated switches with new functionalities.

RESULTS

Development of the nLuc-AFF biosensor

Beginning with the GeNL protein, we duplicated the N terminus of nLuc (residues 1–50; the duplicated sequence is denoted by asterisks) and appended residues 1*–50* to the C terminus of the molecule using a 12-aa linker to generate the nLuc-AFF scaffold. The native (N) and CP frames are shown in Figure 1A. We chose to duplicate this segment because position 50 is at a surface loop that was previously shown to tolerate circular permutation (Verhoef et al., 2016) as well as insertions (Suzuki et al., 2016). To couple the N-to-CP-fold shift to DNA binding, we inserted GCN4 in the surface loop at position 50 of the N frame. In the ligand-free (OFF) state of the switch, GCN4 is predicted to resemble an extended, disordered surface loop in the absence of AP-1. The N fold should tolerate this insertion well, and the OFF state is expected to be green. In the AP-1-bound (ON) state, the length of GCN4 will stretch the 6.3 Å C_α-C_α distance between the ends of the loop, splitting the N frame and triggering the fold shift to the CP frame (Figure 1B). The CP form of nLuc is separated from mNG by 118 aa, 56 of which are a 75 Å rod, and nLuc-AFF is thus expected to emit blue light in the CP frame. We constructed and purified the individual N and CP folds and verified that they were functional green and blue luminescent proteins, respectively (Figure 1C).

The first iteration of nLuc-AFF (Figure S1A; 12-aa linker) exhibited mostly blue luminescence, indicating that it was functional but already in the ON state in the absence of AP-1 (Figure S1C). We consequently destabilized the CP frame by shortening the linker that connected the N- and C termini of the CP frame from 12 to 8, 6, 4, and 2 aa (Table S1). Shorter linkers can destabilize a permuted protein by forcing its termini together, a phenomenon previously demonstrated with barnase (Butler et al., 2009). Shortening the linkers progressively lowered the blue:green ratio as expected, but the population of CP frame was still too large even at 2-aa-linker length (Figure S1C).

To further destabilize the CP fold, we deleted residues 1*–4* from the CP frame (VFTL; the same residues that had been removed from the N frame to make the GeNL variant; Table S1). We then joined the termini of the CP frame with 10, 6, and 4 aa (with the VFTL truncation, the effective linker lengths were 6, 2, and 0 aa). The blue:green ratio diminished with decreasing linker length as before (Figure S1D), and this ratio increased after addition of AP-1 for all three variants (Figure S1E). This increase was largely due to a decrease in green luminescence without an increase in blue luminescence for the 0-aa-linker construct. The 6-aa-linker variant had the best combination of high ratiometric change on AP-1 binding and low background signal, and we used this construct for all further experiments. These results demonstrate that the blue/green populations of the nLuc-AFF sensor can be rationally tuned by adjusting linker length in the CP frame.

Splitting and circularly permuting nLuc typically diminishes its brightness by 10- to 25-fold (Dixon et al., 2016; Verhoef et al., 2016). The emission of nLuc-AFF was 64-fold lower than that of GeNL, as determined by integrating the entire spectrum from 400–600 nm (Figures S2A and S2B). No reduction in mNG fluorescence was observed (Figure S2C). The overall loss of luminescence may have been partly due to the presence of C-terminal truncated proteins, which retain the full mNG domain but may lack luminescence activity. These proteins appeared to have been cleaved by intracellular proteases, and they co-purified with the full-length sensor, possibly by means of their dimerizing GCN4 domains (Figure S3C).

nLuc-AFF retains the affinity of input GCN4 domain with its consensus oligonucleotide

The apparent affinity for the nLuc-AFF for AP-1 was measured by adding various concentrations of AP-1 to a fixed amount of biosensor and measuring the ratiometric change in blue:green emission using a scanning plate reader (dividing intensity at 460 nm by intensity at 520 nm; denoted as L460/L520) or a cell-phone camera (dividing the intensity of the blue channel by the intensity of the green channel). Both methods reported a K_d value of 14.3 ± 3.5 nM (Figures 2A and 2C). We also quantified binding by fluorescence anisotropy of the mNG domain, which reports on the slowdown of molecular tumbling as nLuc-AFF binds AP-1. The fitted K_d value was identical within error (11.6 ± 2.5 nM; Figure S3A), indicating that luminescence turn on results directly from and is limited by DNA binding. These binding affinities are similar to that of the isolated GCN4 peptide for AP-1 (22 ± 9 nM) (Hollenbeck and Oakley, 2000), demonstrating that the GCN4 domain retained full DNA-binding activity in nLuc-AFF. We observed green luminescence even in the presence of fully saturated AP-1 (Figure 1D). This appears to be due to the presence of the aforementioned C-terminally truncated impurities (Figure S3C), which are expected to be either permanently green or nonluminescent.

The turn-on rate of nLuc-AFF was slow when monitored by blue/green luminescence ($t_{1/2}$ = 8.25 ± 0.37 h; Figure S4A). To gain insight into structural events, we mixed nLuc-AFF with AP-1 and tracked binding by fluorescence anisotropy.

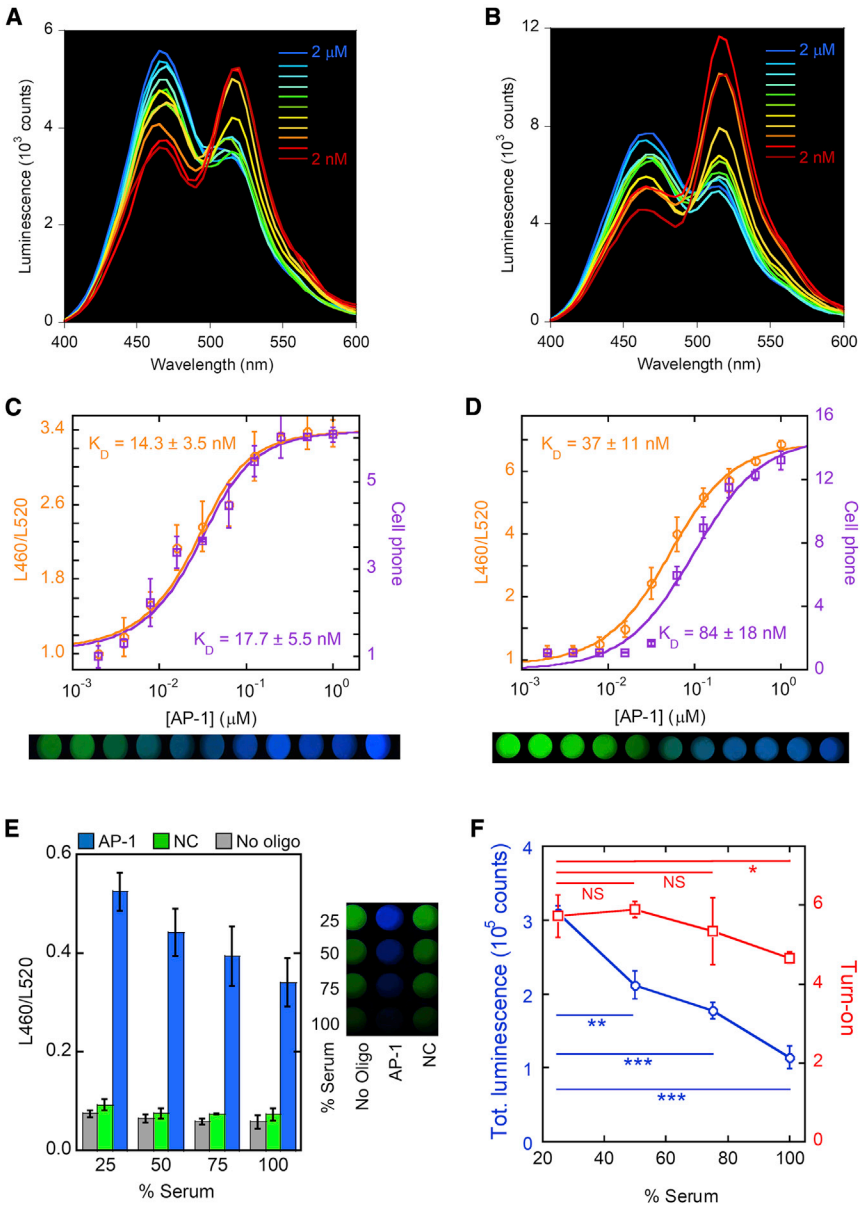

Figure 2. AP-1 binding activates nLuc-AFF in buffer and serum

(A–D) Raw spectra and turn on were quantified in the presence of either 0.1 mg/mL BSA (A and C) or 10% FBS (B and D) by ratio of luminescence at 460 and 520 nm (L460/520; orange) and ratio of blue-to-green channel intensities from cell-phone images (purple), normalized by dividing each point by the biosensor signal at the lowest AP-1 concentration (2 nM). Raw luminescence spectra in (A) and (B) are representative of 4 biological replicates with serial 2-fold dilutions of AP-1 as indicated. The cell-phone images below (C) and (D) are representative of 4 biological replicates and correspond to the same AP-1 dilutions in (A) and (B). Lines in (C) and (D) are best fits to the one-site binding equation. K_D values are average ±SD (n = 3 technical replicates).

(E) AP-1-specific turn on of nLuc-AFF was preserved in serum concentrations up to 100%, as quantified by L460/L520 and cell-phone images. Error bars are SD (n = 3).

(F) Total biosensor luminescence decreased with serum content (blue), but fold turn on (calculated by ratio of L460/L520 values in the presence and absence of AP-1) remained similar. Lines are meant to guide the eye only. Error bars are SD (n = 3), and p values are from an unpaired t test. *p < 0.05; **p < 0.01; ***p < 0.001; ****p < 0.0001; NS, not significant. Sensor concentration was 30 nM in all samples.

Anisotropy increased in two phases, the first of which took place in the ~1 min dead time and the second with a half-time (5.1 ± 1.5 h; Figure S3B) consistent with that of the luminescence change. Conformational capture is the simplest mechanism that can account for this result, although other models cannot be excluded. In this scenario, the observed turn-on rate corresponds to that of the natural interconversion between N and CP folds, with AP-1 binding rapidly to the CP fold and preventing its return to the N fold. This conformational change is expected to be slow because it involves at least partial unfolding (residues 6–50/6*–50* at minimum), and unfolding events tend to be slow in native conditions. However, even though nLuc-AFF was slow to reach completion, a significant signal change could be seen within 1 h (Figure S4B). The phone images also showed a perceptible change in color in this time frame (Figures S4C and S4D). To determine the minimum concentration of biosensor required for detection, we diluted nLuc-AFF in the presence of saturating AP-1 and recorded luminescence on the plate reader. The ratiometric change was detectable down to 7.5 nM (Figure S2D).

It is important for a biosensor to function in dirty environments. This is especially problematic for luciferase-based sensors, as many existing designs show diminished luminescence in serum due to absorbance by extraneous components (Ni et al., 2021). In 10% serum, nLuc-AFF bound to AP-1 with similar affinity (K_D = 37 ± 11 nM; Figures 2B and 2D) as in buffer, as determined by a plate reader and a cell-phone camera. As the serum concentration was raised to 100%, we observed a decrease in overall luminescence intensity (Figure 2E), as expected from serum absorbance, but the change in blue:green ratio due to biosensor activation remained constant within error (Figures 2E and 2F). Raw cell-phone images confirm that the samples were blue in the presence of AP-1 and green in the presence of nonconsensus (NC) DNA (Figure 2E). This result, and the close agreement between the plate-reader and cell-phone-camera data (Figures 2C and 2D), demonstrate that it is possible to quantify the turn-on response using only a cell-phone camera by simply dividing the intensities of the blue and green channels without any image processing.

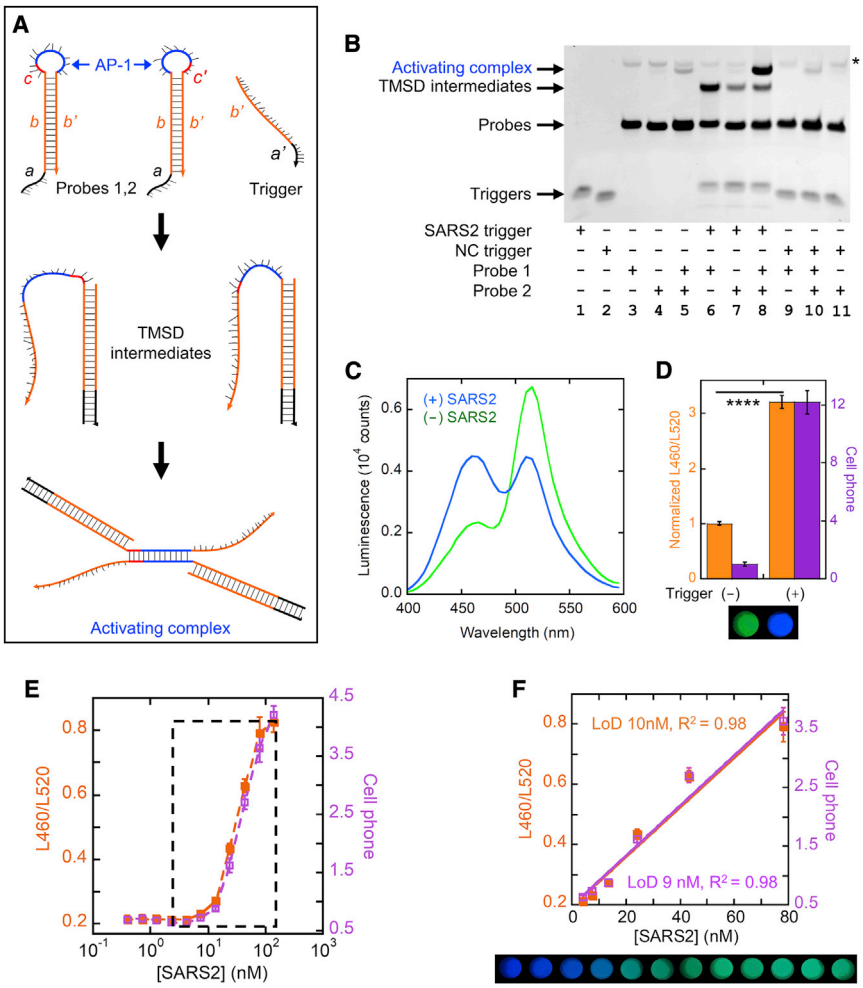

Figure 3. TMSD links an arbitrary DNA sequence to nLuc-AFF switching

(A) For detecting a desired ssDNA or RNA sequence (trigger), two DNA hairpins (probes 1 and 2) were designed with the trigger sequence comprising their stems (*b*) and toeholds (*a*) and the ssAP-1 sequences (blue) embedded in their loops. Probes 1 and 2 contained complementary ssAP-1 and bulge (*c*/*c'*) sequences (see text) in their loops but are otherwise identical. The trigger opens both probes to form the TMSD intermediates, and the ssAP-1 sequences then hybridize to generate the activating complex.

(B) Nondenaturing PAGE detected an intense band of activating complex when probe 1, probe 2, and SARS2 trigger were mixed (lane 8). A faint band of activating complex was observed in mixtures of probe 1, probe 2, and an NC trigger (lane 10) and probe 1 and probe 2 with no trigger (lane 5). The asterisk indicates an impurity that was most likely a probe-1 or -2 dimer.

(C) nLuc-AFF mixed with probes 1 and 2 underwent a green-to-blue luminescence shift in the presence of SARS2 trigger.

(D) The SARS2 trigger sequence turned on nLuc-AFF by 3.2- and 12.4-fold as quantified by L460/L520 ratio and cell-phone images, respectively.

(E) Sensor sensitivity was characterized by mixing 30 nM of nLuc-AFF with 100 nM of probes 1 and 2, followed by SARS2 oligo at the indicated concentrations.

(F) Limit of detection was calculated by fitting the linear response region in (E) (dashed box) to a line (see STAR Methods). Data are plotted as average ±SD (n = 3). Unpaired t tests were performed using the L460/L520 biosensor response. ****$p < 0.0001$.

Compatibility with toehold-mediated strand displacement

Having developed the nLuc-AFF biosensor that is activated by AP-1, our next goal was to couple presentation of the AP-1 sequence to binding of other DNA-sequence inputs. Toehold-mediated strand displacement (TMSD) (Srinivas et al., 2013; Yurke et al., 2000) is a powerful tool that has been extensively used in applications such as signal amplification (Choi et al., 2014, 2018), RNA computation (Green et al., 2017; Kim et al., 2018), and many others. It relies on the ability of an invader strand (single-stranded DNA [ssDNA] or ssRNA) to hybridize to a short ssDNA (the toehold) that overhangs from a double-stranded DNA (dsDNA) stem-loop structure in which the stem and toehold comprise the sequence complementary to that of the invading strand. The invading strand then fully hybridizes with the dsDNA hairpin, displacing the strand of identical sequence to the invader.

We selected a 24-nt sequence from the severe acute respiratory syndrome coronavirus 2 (SARS-CoV-2 [SARS2]) genome to serve as the invading strands for proof of concept. We designed two DNA hairpins in which the 5′ stem and the 5′ toehold consisted of the sequence complementary to the SARS2 oligonucleotide. The hairpins differed only by having the single-stranded AP-1 sequence (ssAP-1) (probe 1) or its complement (probe 2) embedded in their loops. Binding of the SARS2 oligonucleotide opens both probes, exposing their loops. The ssAP-1 sequences then hybridize, generating the activating complex that contains the duplex AP-1 input ligand for nLuc-AFF (Figure 3A). Since AP-1 is a palindromic sequence with a single mismatch in the center, NUPACK (Zadeh et al., 2011) simulations predicted that including ssAP-1 in the loop would extend the stem and make it too stable to be opened by the invading strand. We therefore added a 3-nt "bulge" spacer between the stem and the ssAP-1 loop (*c* and *c'* in Figure 3A). The bulge was predicted to interrupt base stacking at the stem-loop junction, increasing efficiency of hairpin opening.

We evaluated the performance of the designed hairpins by means of native PAGE. When the SARS2 oligonucleotide was incubated with either probe 1 or 2 alone, a new product of higher molecular weight (MW) appeared, corresponding to the expected dimer of the invading strand and opened probe (Figure 3B). We observed a new, larger MW band upon adding the

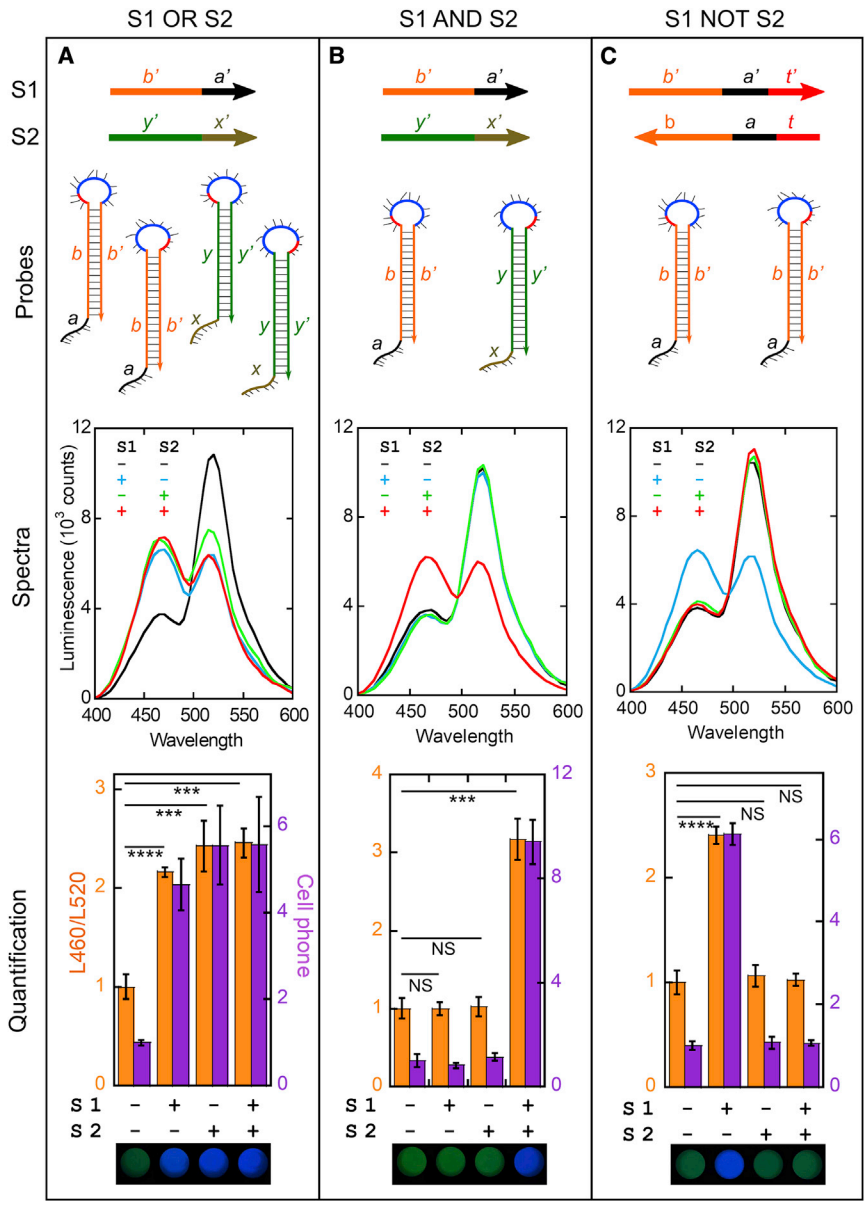

Figure 4. nLuc-AFF provides luminescent output for DNA computation

(A–C) Input DNA strands, computational probes, and biosensor output are shown for OR (A), AND (B), and NOT (C) logic gates. The two input ssDNA strands, S1 and S2, were composed of one of two SARS2 genomic sequences (*b*/*b'* or *y*/*y'*) and a toehold (*a*/*a'* or *x*/*x'*). For the NOT condition, the S1 toehold was extended by 6 nt (*t'*), and S2 was an exact complement of S1. The additional 6 nt helps clamp S1 and S2 together, reducing fraying of the toehold in the S1/S2 complex that would result in probe invasion and nonspecific turn on of the sensor (Yin et al., 2008). The computational DNA probes were hairpins consisting of the SARS2 recognition sequences in their stems, complementary ssAP-1 sequences (blue) and bulge oligonucleotides (red) in their loops, and toehold sequences extending from the stems. These probes were kept constant in all four conditions of the logic gates. OR, AND, and NOT outputs were established by mixing S1 and S2 in all four combinations and recording luminescence changes by plate reader (middle) or cell-phone camera (bottom images) in which green and blue indicate OFF and ON states, respectively. Sensor response was quantified by L460/L520 (orange bars, left y axis) and by the ratio of blue and green channels in the cell-phone image (purple bars, right y axis). Data were normalized to the condition where neither S1 nor S2 were present. Spectra are representative of three to four technical replicates. Error bars are SD (n = 3). Unpaired t tests were performed using the L460/L520 biosensor response. ***p < 0.001; ***p < 0.0001; NS, not significant.

SARS2 oligonucleotide to both probes, consistent with formation of the activating complex.

Biosensor activation was tested by mixing nLuc-AFF with the two probes in the presence or absence of the SARS2 oligonucleotide. We detected a decrease in green luminescence and an increase in blue luminescence only in the presence of the SARS2 strand (Figure 3C). L460/L520 revealed a 3.2-fold change in biosensor turn on along with a color change visible by cell-phone camera (blue:green ratio change of 12.2) (Figure 3D). This finding, along with the PAGE data, verify that the activating AP-1 duplex is formed from two hairpins only in the presence of the initiating SARS2 sequence. The limit of detection (LoD) was in close agreement both by cell-phone camera (9 nM) and plate reader (10 nM; Figures 3E and 3F). Although nLuc-AFF is not sensitive enough to act as a SARS-CoV-2 biosensor as is, its sensitivity can be increased by incorporating DNA pre-amplification steps such as loop-mediated isothermal amplification (LAMP) or recombinase polymerase amplification, a strategy that is employed in most Cas12- (Broughton et al., 2020; Kaminski et al., 2021; Sun et al., 2021) and Cas13-based (Arizti-Sanz et al., 2020; Joung et al., 2020; Patchsung et al., 2020) sensing platforms. These results demonstrate that our biosensor can be used with TMSD-based DNA devices.

Compatibility with DNA-based logic devices

To demonstrate the adaptability of our system, we applied it as a logic gate to process two ssDNA inputs. The first input strand (S1) was the same SARS2 oligonucleotide in Figure 3, and the second input strand (S2) was identical except it bore a different 24-nt SARS2 genomic sequence. Using the approach described above, we then designed three separate sets of computational DNA probes to serve as logic gates, turning on via TMSD if (1) either S1 or S2 is present (OR condition), (2) both S1 and S2 are present (AND condition), or (3) S1 is present and S2 is not present (NOT condition). Input and probe oligonucleotides are shown in Figure 4.

The S1 OR S2 logic gate (Figure 4A) was composed of two sets of hairpin pairs, one recognizing S1 and the other recognizing S2, each independently capable of opening and generating a separate activating complex. In agreement, we observed a large color shift when either of the two input strands was added to the biosensor-hairpin mix (Figure 4A). The S1 AND S2 gate (Figure 4B) contained a single probe that recognizes S1 and another that recognizes S2, such that both SARS2 sequences must be present to generate the activating complex. As expected, the biosensor was not activated by either S1 or S2 alone, and the addition of both inputs gave rise to a large color shift (Figure 4B, bottom). The S1 NOT S2 logic gate (Figure 4C) consisted of a pair of hairpins that both recognize S1 and generate the activating complex upon binding. S2 was designed to base pair with S1 and thus inhibit S1 from initiating TMSD. S2 alone did not activate the biosensor-hairpin mix, and S1 alone gave rise to a large spectral shift, both as predicted (Figure 4C). When we added S1 and S2, the blue:green ratio diminished to the same value that was observed without any inputs, satisfying the S1 NOT S2 condition.

Compatibility with DNA aptamers

Sensing analytes of biological or clinical interest is a major goal of biosensor development. Many protein-based switches, including nLuc-AFF, employ natural, evolved, or *de-novo*-designed protein domains to bind the analytes and activate the output domains through allosteric mechanisms. This approach is powerful, but it is limited by the dual challenge of generating new binding domains that recognize the target of interest as well as undergo a large conformational change that transmits the binding signal to the output domain. DNA- and RNA-based aptamers provide a solution to the first challenge. Aptamers with high affinity and specificity for an arbitrary analyte can be obtained with relative ease by systematic evolution of ligands by exponential enrichment (SELEX)-based screening of large DNA libraries. The aptamers can then be derivatized with chemical dyes and molecular beacons for fluorescent output (Wang et al., 2011) or attached to surfaces for detection by field-effect transistor devices (Nakatsuka et al., 2018). It is not obvious, however, how the binding readout of aptamers can be expanded to include biological activities provided by protein- and enzyme-based output domains.

Our nLuc-AFF system addresses the above limitation by acting as a "universal" adapter that connects aptamer/analyte binding to bioluminescence. It is universal in the respect that it is designed to work with existing aptamers without any changes to nLuc-AFF or chemical derivatization/surface attachment of the aptamer. The only modification is the addition of an oligonucleotide sequence to either the 5′ or 3′ end of the aptamer. To test that assertion, we sought to create a luminescent biosensor for serotonin using an aptamer that was developed elsewhere (Nakatsuka et al., 2018). We modified the serotonin aptamer (green and red in Figure 5A) by adding to its 5′ end a sequence consisting of ssAP-1 (blue) and an additional "clamp" sequence (pink) that is complementary to first 8 nt of the aptamer (red). In the absence of ligand, the aptamer structure is unstable, and the red sequence base pairs to the clamp, which, along with the blue sequence, forms the stem of a stable hairpin that prevents ssAP-1 from activating the biosensor (Figure 5A, left structure). When the aptamer binds serotonin, it folds and reclaims the red sequence, opening the hairpin and exposing the ssAP-1 sequence in the loop (Figure 5A, middle structure). This is essentially the DNA analog of the AFF mechanism. A second ssDNA oligonucleotide (naked AP-1) consisting of the sequence complementary to ssAP-1 and a truncated clamp (4 nt) is added to generate duplex AP-1 and activate nLuc-AFF (Figure 5A, right structure). NUPACK was used to determine the optimal clamp lengths in the modified aptamer (to form a stable hairpin in the absence of ligand) and in naked AP-1 (to minimize false activation of the aptamer) (Figure S5A).

We used native PAGE to establish that the modified aptamer did not bind naked AP-1 in the absence of serotonin. The aptamer alone ran as an intense, faster-migrating band and a faint, slower-migrating band (Figure S5B). The slower species is likely a dimer, which is expected due to its largely palindromic AP-1 sequence along with the hairpin that protects it. We did not observe any additional products when naked AP-1 was added to the aptamer in the absence of serotonin. With serotonin, a new band was observed that likely corresponds to the activating complex depicted in Figure 5A.

Having determined that a 1:1 ratio of aptamer:naked AP-1 yielded optimal results (Figures S5C–S5G), we evaluated sensor performance by adding 10 μM serotonin to samples containing 250 nM aptamer, 250 nM naked AP-1, and 30 nM nLuc-AFF. We observed a 1.4-fold ratiometric change in L460/L520 (Figures 5B and 5C) and no change when the sensor was mixed with serotonin in the absence of aptamer (Figure S5F). The color change was visible by cell-phone camera (Figure 5B inset), with an average of a 2-fold biosensor activation (Figure 5C).

We next asked if our strategy was generalizable to other aptamers. We modified a well-characterized ATP aptamer (Huizenga and Szostak, 1995) to contain the ssAP-1 and clamp sequences using the approach described above, except we appended those nucleotides to the 3′ end of the ATP aptamer. As with the serotonin aptamer, we detected a spectral shift upon addition of 2 mM ATP, with a 1.3-fold increase in L460/L520 and a 1.9-fold change from the cell-phone image (Figures 5D and 5E). These results suggest that our design can be applied to existing aptamers to generate new luminescent sensors for a variety of small molecules and proteins.

Detection of serotonin is of considerable clinical interest. In conditions such as heparin-induced thrombocytopenia (HIT) and catecholamine-secreting carcinoid tumors, accurate quantification of platelet and serum serotonin can help aid diagnosis. HIT is a severe hypercoagulable condition with up to a 30% mortality rate (Stoll et al., 2018). Although other clinical tests such as anti-platelet factor 4 (PF4) antibody titer are routinely performed, sensitive diagnosis relies on serotonin-release assay (SRA) (Nicolas et al., 2022). However, most healthcare settings source it to other facilities, causing large turnaround times. Our method provides an alternative to current methods used to perform SRA in low-resource settings. The apparent affinity of the aptamer-biosensor (0.37 ± 0.07 μM; Figure S5H) suggests that for HIT, levels of serotonin in healthy (0.11–0.36 μM) and diseased (1.5–46 μM) patients (Harenberg et al., 2000) can be distinguished. Moreover, SRAs can also be used to diagnose vaccine-induced thrombocytopenia.

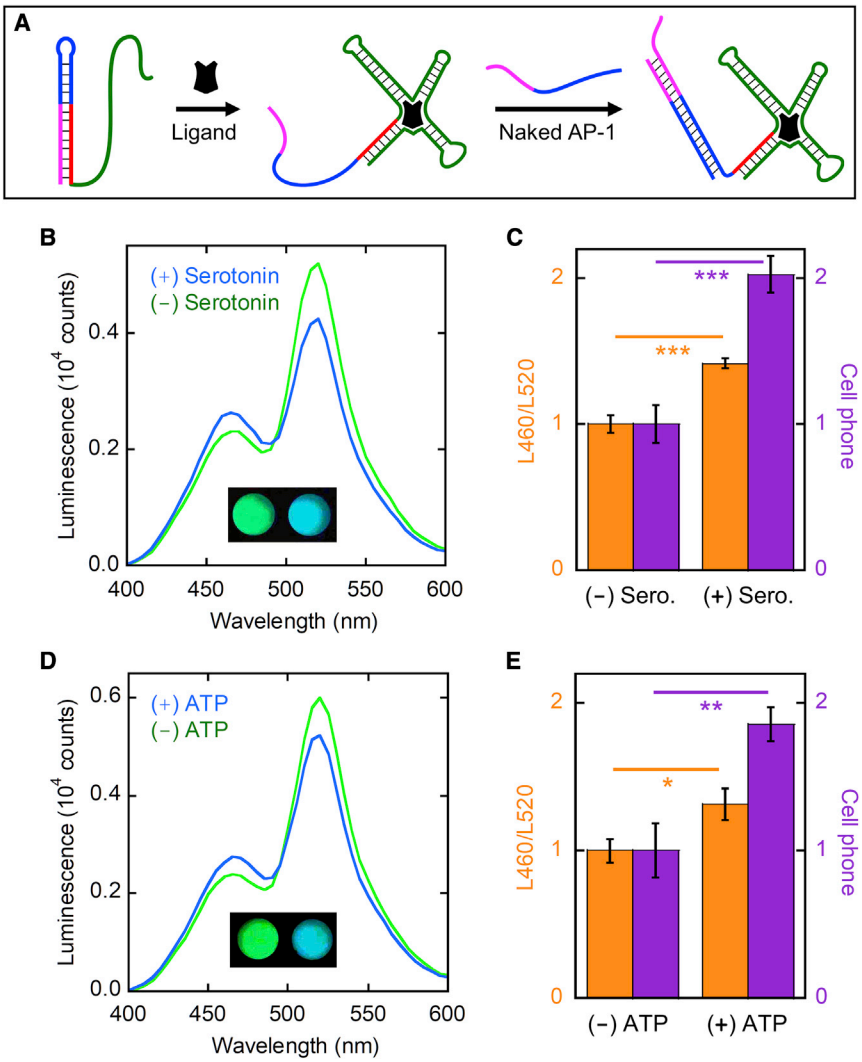

Figure 5. Small-molecule activation of nLuc-AFF via DNA aptamers

(A) In the left structure, the parental DNA aptamer (green and red) was modified by appending it to the ssAP-1 sequence (blue) and a clamp sequence (pink) that was complementary to the red sequence. Pairing of the pink and red strands stabilizes ssAP-1 in a hairpin structure, rendering it incapable of activating nLuc-AFF. Ligand binding induces the aptamer to fold, which displaces the clamp sequence and disrupts the ssAP-1 hairpin (center structure). The exposed ssAP-1/clamp sequence is then able to pair with an oligonucleotide consisting of the complementary ssAP-1 sequence and a portion of the clamp (naked AP-1; blue and pink strand). The resulting complex (right structure) contains the duplex AP-1 sequence that activates the biosensor.

(B and D) Mixing 10 μM serotonin and 2 mM ATP with their respective aptamers, naked ssAP-1, and nLuc-AFF triggered a green-to-blue luminescence change as detected by emission spectra and raw cell-phone pictures (insets).

(C and E) Quantifying sensor response by L460/L520 or ratio of blue/green channels from cell-phone images revealed 2.7- and 3.0-fold turn on (respectively) for the serotonin aptamer and 3.2- and 3.5-fold turn on (respectively) for the ATP aptamer. For this calculation, the signal from the biosensor with no aptamers or ligands present was subtracted from the observed signal, and the resulting values were normalized to the control with no ligand present. Unpaired t tests were performed for statistical significance. *$p < 0.05$. **$p < 0.01$, ***$p < 0.001$.

DISCUSSION

In this study, we developed an enzymatic biosensor that was activated by different DNA inputs. The same nLuc-AFF protein can be paired with different DNA technologies for use in several applications. TMSD converts an arbitrary nucleotide sequence into the AP-1 input for the sensor for the purpose of detecting a DNA/RNA sequence of choice or creating DNA-based computational devices with luminescent readout. Aptamers extend the potential targets of the nLuc-AFF biosensor to small molecules, metabolites, and proteins.

How does nLuc-AFF compare to existing sensor designs? Many of the basic functions of nLuc-AFF can be performed by DNA tools alone, for instance, by one of the hairpins or aptamers in this study modified with fluorescent donor and quencher groups at two positions that change proximity on binding. Bioluminescent sensors offer the benefits of genetic encodability as well as the superior sensitivity and simplicity of luminescence detection, although a substrate (furimazine or coelenterazine) is required, and modifying luciferase often reduces its brightness. There are several examples of successful luciferase-based sensors. Split luciferase systems such as NanoBiT (Dixon et al., 2016) bisect nLuc into fragments (large BiT and small BiT), each of which is fused to proteins that bind ligand in a sandwich-type interaction (Glasgow et al., 2019; Quijano-Rubio et al., 2021; Xu et al., 2020) or to a single protein that undergoes an open-to-closed conformational change (Du et al., 2019; Hossain et al., 2018). The ternary complex increases the local concentration of nLuc fragments, resulting in complementation and luminescence turn on. General nonidealities with bimolecular sensors are the need to express two proteins in cells, their intensity-only signal change, and the dependence of response on sensor concentration (due to fragment complementation in the absence of ligand). Fragment pairs with a variety of intrinsic affinities, however, have been generated to minimize the latter concern (Dixon et al., 2016). Merkx and coworkers developed an unimolecular and ratiometric version of this design in which large and small BiT were connected via a flexible linker that contained epitopes for a monoclonal antibody at both ends, as well as a chemical dye, resulting in efficient red BRET (Ni et al., 2019). Binding of the epitopes to the arms of an antibody caused the linker to elongate, causing small BiT to detach and become replaced by a second small BiT (that was also fused to the large

BiT), reverting nLuc luminescence to blue. The same researchers also created a ''BRET-beacon'' with functionality similar to that of nLuc-AFF (Engelen et al., 2017). They conjugated nLuc to an ssDNA oligonucleotide that hybridized to a DNA tool that bore a recognition sequence in a loop and a Cy3 acceptor dye at its terminus. Binding of target ssDNA/ssRNA converted the loop to a long helix, distancing Cy3 from nLuc and reducing BRET. Winssinger and colleagues reported another semisynthetic nLuc-peptide nucleic acid (PNA) hybrid that uses TMSD to sense DNA and RNA sequences by displacing a complementary strand with a nLuc inhibitor and turning on luminescence (Chang et al., 2020).

The chief merit of nLuc-AFF is how it achieves plug-and-play capability. Some of the sensor designs described above require their recognition domains to be modified or replaced in order to recognize new ligands. This is challenging for small/large-BiT complementation systems, as finding or engineering protein partners that come together only in the presence of the target can be difficult. The small-BiT intramolecular exchange sensor excels at detecting antibodies, but the bidentate interaction mechanism may not readily translate to other ligands. The BRET-beacon and nLuc-PNA designs are fully modular: one simply needs to attach different recognition oligonucleotides to the nLuc output domain. nLuc-AFF does not employ chemical coupling, and more importantly, the same nLuc-AFF protein can be used to detect arbitrary DNA/RNA sequences and small molecules or proteins for which aptamers exist. Only the DNA hairpins or aptamers need to be modified to transform the DNA/RNA sequence or small molecule/protein to the activating AP-1 signal, respectively. Similarly, the DNA tools described in this study can be used to convert a new target DNA sequence into the sequence recognized by a BRET-beacon sensor, without modifying the latter.

The nLuc-AFF switch developed here has several notable attributes. It retains the DNA-binding affinity and luminescent properties of the parent GCN4 and nLuc proteins, respectively, and it is not falsely activated by decoy DNA sequences. Its ratiometric output enables quantification by cell phone by simply recording an RGB image and dividing the raw intensity of the blue channel by that of the green channel. The dual-color output establishes an internal normalization of intensity that makes it possible to quantify cell-phone images. Finally, nLuc-AFF stands out from some other luciferase-based platforms in that it performs well in serum without needing a secondary luminescent protein to calibrate for signal loss, opening the door to its potential use in clinical samples.

Taking a broader perspective, the AFF mechanism is distinct because it has the potential to regulate proteins with activities other than luminescence. The unimolecular luciferase-based sensors discussed above operate on a principle that is idiosyncratic to light-emitting proteins: the dependence of luminescence (or fluorescence) emission on distance to an acceptor in the form of BRET (or fluorescence resonance energy transfer [FRET]). Ligand binding alters this distance without changing the structure or function of nLuc. By contrast, AFF introduces a ligand-induced conformational change into a protein that results in one set of residues being replaced by another. This fold shift has been used to switch on and off nuclease activity (Karchin et al., 2017; Mitrea et al., 2010), calcium and ribose binding (Karchin et al., 2017; Stratton et al., 2008), and fluorescence (Do and Boxer, 2013; John et al., 2022).

Limitations of this study

The foremost limitation of our current design is its slow turn-on half-time (8.25 h), which can be several orders of magnitude longer than that of split nLuc sensors (Ni et al., 2019). Experimental (John et al., 2022; Stratton and Loh, 2010) and computational (DeGrave et al., 2018) studies of other AFF-modified proteins suggest that slow switching is due to a large kinetic barrier to the unfolding of the N frame. Introducing mutations to destabilize the N fold can accelerate the overall switching rate. Care must be taken to preserve the thermodynamic balance between N and CP folds, and this can be accomplished by introducing the mutation in the region shared by the two folds (residues 51–171; Figure 1B) or by placing identical mutations in each of the duplicated segments. Destabilizing mutations can often be predicted by structural inspection or computational methods, but these do not always accelerate unfolding rates. A more rational approach is to simulate the AFF conformational change using weighted ensemble methods and identify amino acids that, when mutated, destabilize the N and CP folds but not the transition-state ensemble (DeGrave et al., 2018).

The second limitation arises from the palindromic nature of the AP-1 sequence that activates the sensor. Our methods incorporate the activating sequence into various DNA structures, where it is cryptic until the triggering event (TMSD or ligand binding to aptamer) exposes it for hybridizing with its complement. In the case of TMSD, the DNA structures are hairpins, and introducing the palindromic ssAP-1 sequence into the loop can affect their metastability. Moreover, an unprotected ssAP-1 sequence (such as that in the complementary activating strand in our aptamer experiments) can homodimerize, giving rise to nonspecific activation. What is needed to resolve this problem is a DNA-binding protein that recognizes a nonpalindromic sequence, has a reasonably long N-to-C distance ($\geq$20 Å), and can be engineered to be unstable in the absence of DNA. Zinc-finger (ZnF) DNA-binding domains may be able to serve this purpose, as they are flexible without DNA (Tochio et al., 2015) and take on long, stable structures on DNA binding akin to that of GCN4 (Christy et al., 1988; Pavletich and Pabo, 1991). Another advantage of ZnF domains is their high affinity toward specific target sequences. Since, as shown in this study, the sensitivity of a biosensor is greatly dependent on the binding affinity of the input domain, substituting ZnF for GCN4 will also help lower the LoD of nLuc-AFF. It may also be possible to use SELEX methods to identify an ssDNA aptamer that binds specifically to an altogether different input domain, i.e., a small protein that meets the distance and stability requirements mentioned above. This aptamer sequence would take the place of AP-1 and eliminate the need for the complementary activating strand.

The third limitation of our system is its modest ratiometric output when used with aptamers. We believe this is due primarily to false activation by the naked AP-1 strand and secondarily to the presence of always-green impurities. Both problems can be solved by employing a DNA-recognition domain other than GCN4, as discussed above.

STAR★METHODS

Detailed methods are provided in the online version of this paper and include the following:

- KEY RESOURCES TABLE
- RESOURCE AVAILABILITY
  - Lead contact
  - Materials availability
  - Data and code availability
- METHOD DETAILS
  - Gene construction and protein purification
  - Luminescence measurements and image processing
  - Biosensor performance characterization
  - Oligonucleotide design and purification
  - Toehold mediated strand displacement and logic gate experiments
  - Validation of nLuc-AFF with DNA aptamers
  - Serotonin aptamer equilibrium binding
  - Biosensor turn-on kinetics
  - Determination of the limit of detection
  - AP-1 binding by fluorescence anisotropy
- QUANTIFICATION AND STATISTICAL ANALYSIS

SUPPLEMENTAL INFORMATION

Supplemental information can be found online at https://doi.org/10.1016/j.crmeth.2022.100202.

ACKNOWLEDGMENTS

We thank Dr. Jeung-Hoi Ha for discussions. This work was supported by NIH grant R01GM115762 to S.N.L.

AUTHOR CONTRIBUTIONS

Conceptualization, H.S. and S.N.L; methodology, H.S. and S.N.L; validation, formal analysis, and investigation, H.S. and S.N.L.; writing – original draft, H.S.; writing – review & editing, H.S. and S.N.L.; visualization, H.S. and S.N.L.; funding acquisition, S.N.L.

DECLARATION OF INTERESTS

The authors declare no competing interests.

Received: December 27, 2021
Revised: February 24, 2022
Accepted: March 28, 2022
Published: April 18, 2022

REFERENCES

Arizti-Sanz, J., Freije, C.A., Stanton, A.C., Petros, B.A., Boehm, C.K., Siddiqui, S., Shaw, B.M., Adams, G., Kosoko-Thoroddsen, T.-S.F., Kemball, M.E., et al. (2020). Streamlined inactivation, amplification, and Cas13-based detection of SARS-CoV-2. Nat. Commun. *11*, 5921. https://doi.org/10.1038/s41467-020-19097-x.

Biewenga, L., Rosier, B.J.H.M., and Merkx, M. (2020). Engineering with NanoLuc: a playground for the development of bioluminescent protein switches and sensors. Biochem. Soc. Trans. *48*, 2643–2655. https://doi.org/10.1042/BST20200440.

Bracaglia, S., Ranallo, S., Plaxco, K.W., and Ricci, F. (2021). Programmable, multiplexed DNA circuits supporting clinically relevant, electrochemical antibody detection. ACS Sens. *6*, 2442–2448. https://doi.org/10.1021/acssensors.1c00790.

Broughton, J.P., Deng, X., Yu, G., Fasching, C.L., Servellita, V., Singh, J., Miao, X., Streithorst, J.A., Granados, A., Sotomayor-Gonzalez, A., et al. (2020). CRISPR–Cas12-based detection of SARS-CoV-2. Nat. Biotechnol., 1–5. https://doi.org/10.1038/s41587-020-0513-4.

Butler, J.S., Mitrea, D.M., Mitrousis, G., Cingolani, G., and Loh, S.N. (2009). Structural and thermodynamic analysis of a conformationally strained circular permutant of barnase. Biochemistry *48*, 3497–3507. https://doi.org/10.1021/bi900039e.

Chandrasekaran, A.R., and Halvorsen, K. (2021). DNA-based smart reagent for detecting Alzheimer's associated MicroRNAs. ACS Sens. *6*, 3176–3181. https://doi.org/10.1021/acssensors.1c01567.

Chang, D., Kim, K.T., Lindberg, E., and Winssinger, N. (2020). Smartphone DNA or RNA sensing using semisynthetic luciferase-based logic device. ACS Sens. *5*, 807–813. https://doi.org/10.1021/acssensors.9b02454.

Choi, H.M.T., Beck, V.A., and Pierce, N.A. (2014). Next-generation in situ hybridization chain reaction: higher gain, lower cost, greater durability. ACS Nano *8*, 4284–4294. https://doi.org/10.1021/nn405717p.

Choi, H.M.T., Schwarzkopf, M., Fornace, M.E., Acharya, A., Artavanis, G., Stegmaier, J., Cunha, A., and Pierce, N.A. (2018). Third-generation in situ hybridization chain reaction: multiplexed, quantitative, sensitive, versatile, robust. Development *145*, dev165753. https://doi.org/10.1242/dev.165753.

Christy, B.A., Lau, L.F., and Nathans, D. (1988). A gene activated in mouse 3T3 cells by serum growth factors encodes a protein with "zinc finger" sequences. Proc. Natl. Acad. Sci. U S A *85*, 7857–7861. https://doi.org/10.1073/pnas.85.21.7857.

DeGrave, A.J., Ha, J.-H., Loh, S.N., and Chong, L.T. (2018). Large enhancement of response times of a protein conformational switch by computational design. Nat. Commun. *9*, 1–9. https://doi.org/10.1038/s41467-018-03228-6.

Dixon, A.S., Schwinn, M.K., Hall, M.P., Zimmerman, K., Otto, P., Lubben, T.H., Butler, B.L., Binkowski, B.F., Machleidt, T., Kirkland, T.A., et al. (2016). NanoLuc complementation reporter optimized for accurate measurement of protein interactions in cells. ACS Chem. Biol. *11*, 400–408. https://doi.org/10.1021/acschembio.5b00753.

Do, K., and Boxer, S.G. (2013). GFP variants with alternative β-strands and their application as light-driven protease sensors: a tale of two tails. J. Am. Chem. Soc. *135*, 10226–10229. https://doi.org/10.1021/ja4037274.

Du, Y., Hu, H., Pei, X., Du, K., and Wei, T. (2019). Genetically encoded FapR-NLuc as a biosensor to determine Malonyl-CoA in situ at subcellular scales. Bioconjug. Chem. *30*, 826–832. https://doi.org/10.1021/acs.bioconjchem.8b00920.

Engelen, W., van de Wiel, K.M., Meijer, L.H.H., Saha, B., and Merkx, M. (2017). Nucleic acid detection using BRET-beacons based on bioluminescent protein-DNA hybrids. Chem. Commun. (Camb) *53*, 2862–2865. https://doi.org/10.1039/c6cc10032e.

England, C.G., Ehlerding, E.B., and Cai, W. (2016). NanoLuc: a small luciferase is brightening up the field of bioluminescence. Bioconjug. Chem. *27*, 1175–1187. https://doi.org/10.1021/acs.bioconjchem.6b00112.

Glasgow, A.A., Huang, Y.-M., Mandell, D.J., Thompson, M., Ritterson, R., Loshbaugh, A.L., Pellegrino, J., Krivacic, C., Pache, R.A., Barlow, K.A., et al. (2019). Computational design of a modular protein sense-response system. Science *366*, 1024–1028. https://doi.org/10.1126/science.aax8780.

Green, A.A., Kim, J., Ma, D., Silver, P.A., Collins, J.J., and Yin, P. (2017). Complex cellular logic computation using ribocomputing devices. Nature *548*, 117–121. https://doi.org/10.1038/nature23271.

Guo, Z., Parakra, R.D., Xiong, Y., Johnston, W.A., Walden, P., Edwardraja, S., Moradi, S.V., Ungerer, J.P.J., Ai, H., Phillips, J.J., and Alexandrov, K. (2022). Engineering and exploiting synthetic allostery of NanoLuc luciferase. Nat. Commun. *13*, 789. https://doi.org/10.1038/s41467-022-28425-2.

Ha, J.H., Butler, J.S., Mitrea, D.M., and Loh, S.N. (2006). Modular enzyme design: regulation by mutually exclusive protein folding. J. Mol. Biol. *357*, 1058–1062. https://doi.org/10.1016/j.jmb.2006.01.073.

Hall, M.P., Unch, J., Binkowski, B.F., Valley, M.P., Butler, B.L., Wood, M.G., Otto, P., Zimmerman, K., Vidugiris, G., Machleidt, T., et al. (2012). Engineered luciferase reporter from a deep sea shrimp utilizing a novel imidazopyrazinone substrate. ACS Chem. Biol. *7*, 1848–1857. https://doi.org/10.1021/cb3002478.

Harenberg, J., Huhle, G., Giese, Ch., Wang, L.C., Feuring, M., Song, X.H., and Hoffmann, U. (2000). Determination of serotonin release from platelets by enzyme immunoassay in the diagnosis of heparin-induced thrombocytopenia. Br. J. Haematol. *109*, 182–186. https://doi.org/10.1046/j.1365-2141.2000.01966.x.

Hollenbeck, J.J., and Oakley, M.G. (2000). GCN4 binds with high affinity to DNA sequences comtaining a single half-site. Biochemistry *39*, 6380–6389.

Hossain, M.N., Suzuki, K., Iwano, M., Matsuda, T., and Nagai, T. (2018). Bioluminescent low-affinity Ca2+ indicator for ER with multicolor calcium imaging in single living cells. ACS Chem. Biol. *13*, 1862–1871. https://doi.org/10.1021/acschembio.7b01014.

Huizenga, D.E., and Szostak, J.W. (1995). A DNA aptamer that binds adenosine and ATP. Biochemistry *34*, 656–665. https://doi.org/10.1021/bi00002a033.

John, A.M., Sekhon, H., Ha, J.-H., and Loh, S.N. (2022). Engineering a fluorescent protein color switch using entropy-driven β-strand exchange. ACS Sens. *7*, 263–271. https://doi.org/10.1021/acssensors.1c02239.

Joung, J., Ladha, A., Saito, M., Kim, N.-G., Woolley, A.E., Segel, M., Barretto, R.P.J., Ranu, A., Macrae, R.K., Faure, G., et al. (2020). Detection of SARS-CoV-2 with SHERLOCK one-Pot testing. N. Engl. J. Med. *383*, 1492–1494. https://doi.org/10.1056/NEJMc2026172.

Kaminski, M.M., Abudayyeh, O.O., Gootenberg, J.S., Zhang, F., and Collins, J.J. (2021). CRISPR-based diagnostics. Nat. Biomed. Eng. *5*, 643–656. https://doi.org/10.1038/s41551-021-00760-7.

Karchin, J.M., Ha, J.-H., Namitz, K.E., Cosgrove, M.S., and Loh, S.N. (2017). Small molecule-induced domain swapping as a mechanism for controlling protein function and assembly. Sci. Rep. *7*, 44388. https://doi.org/10.1038/srep44388.

Kim, J., Yin, P., and Green, A.A. (2018). Ribocomputing: cellular logic computation using RNA devices. Biochemistry *57*, 883–885. https://doi.org/10.1021/acs.biochem.7b01072.

Krishnan, Y., Zou, J., and Jani, M.S. (2020). Quantitative imaging of biochemistry in situ and at the nanoscale. ACS Cent. Sci. *6*, 1938–1954. https://doi.org/10.1021/acscentsci.0c01076.

Langan, R.A., Boyken, S.E., Ng, A.H., Samson, J.A., Dods, G., Westbrook, A.M., Nguyen, T.H., Lajoie, M.J., Chen, Z., Berger, S., et al. (2019). De novo design of bioactive protein switches. Nature *572*, 205–210. https://doi.org/10.1038/s41586-019-1432-8.

Lavín, Á., de Vicente, J., Holgado, M., Laguna, M.F., Casquel, R., Santamaría, B., Maigler, M.V., Hernández, A.L., and Ramírez, Y. (2018). On the determination of uncertainty and limit of detection in label-free biosensors. Sensors (Basel) *18*, 2038. https://doi.org/10.3390/s18072038.

Madsen, M., and Gothelf, K.V. (2019). Chemistries for DNA nanotechnology. Chem. Rev. *119*, 6384–6458. https://doi.org/10.1021/acs.chemrev.8b00570.

Mitrea, D.M., Parsons, L., and Loh, S.N. (2010). Engineering an artificial zymogen by alternate frame protein folding. Proc. Natl. Acad. Sci. U S A *107*, 2824–2829.

Nakatsuka, N., Yang, K.-A., Abendroth, J.M., Cheung, K.M., Xu, X., Yang, H., Zhao, C., Zhu, B., Rim, Y.S., Yang, Y., et al. (2018). Aptamer-field-effect transistors overcome Debye length limitations for small-molecule sensing. Science *362*, 319–324. https://doi.org/10.1126/science.aao6750.

Ni, Y., Arts, R., and Merkx, M. (2019). Ratiometric bioluminescent sensor proteins based on intramolecular split luciferase complementation. ACS Sens. *4*, 20–25. https://doi.org/10.1021/acssensors.8b01381.

Ni, Y., Rosier, B.J.H.M., van Aalen, E.A., Hanckmann, E.T.L., Biewenga, L., Pistikou, A.-M.M., Timmermans, B., Vu, C., Roos, S., Arts, R., et al. (2021). A plug-and-play platform of ratiometric bioluminescent sensors for homogeneous immunoassays. Nat. Commun. *12*, 4586. https://doi.org/10.1038/s41467-021-24874-3.

Nicolas, D., Nicolas, S., Hodgens, A., and Reed, M. (2022). Heparin induced thrombocytopenia. In StatPearls (StatPearls Publishing).

Ong, L.L., Hanikel, N., Yaghi, O.K., Grun, C., Strauss, M.T., Bron, P., Lai-Kee-Him, J., Schueder, F., Wang, B., Wang, P., et al. (2017). Programmable self-assembly of three-dimensional nanostructures from 10,000 unique components. Nature *552*, 72–77. https://doi.org/10.1038/nature24648.

O'Shea, E.K., Klemm, J.D., Kim, P.S., and Alber, T. (1991). X-ray structure of the GCN4 leucine zipper, a two-stranded, parallel coiled coil. Science *254*, 539–544.

Patchsung, M., Jantarug, K., Pattama, A., Aphicho, K., Suraritdechachai, S., Meesawat, P., Sappakhaw, K., Leelahakorn, N., Ruenkam, T., Wongsatit, T., et al. (2020). Clinical validation of a Cas13-based assay for the detection of SARS-CoV-2 RNA. Nat. Biomed. Eng. *4*, 1140–1149. https://doi.org/10.1038/s41551-020-00603-x.

Pavletich, N.P., and Pabo, C.O. (1991). Zinc finger-DNA recognition: crystal structure of a Zif268-DNA complex at 2.1 A. Science *252*, 809–817. https://doi.org/10.1126/science.2028256.

Quijano-Rubio, A., Yeh, H.-W., Park, J., Lee, H., Langan, R.A., Boyken, S.E., Lajoie, M.J., Cao, L., Chow, C.M., Miranda, M.C., et al. (2021). De novo design of modular and tunable protein biosensors. Nature *591*, 482–487. https://doi.org/10.1038/s41586-021-03258-z.

Saka, S.K., Wang, Y., Kishi, J.Y., Zhu, A., Zeng, Y., Xie, W., Kirli, K., Yapp, C., Cicconet, M., Beliveau, B.J., et al. (2019). Immuno-SABER enables highly multiplexed and amplified protein imaging in tissues. Nat. Biotechnol. *37*, 1080–1090. https://doi.org/10.1038/s41587-019-0207-y.

Schneider, C.A., Rasband, W.S., and Eliceiri, K.W. (2012). NIH Image to ImageJ: 25 years of image analysis. Nat. Methods *9*, 671–675. https://doi.org/10.1038/nmeth.2089.

Srinivas, N., Ouldridge, T.E., Sulc, P., Schaeffer, J.M., Yurke, B., Louis, A.A., Doye, J.P.K., and Winfree, E. (2013). On the biophysics and kinetics of toehold-mediated DNA strand displacement. Nucleic Acids Res. *41*, 10641–10658. https://doi.org/10.1093/nar/gkt801.

Stoll, F., Gödde, M., Leo, A., Katus, H.A., and Müller, O.J. (2018). Characterization of hospitalized cardiovascular patients with suspected heparin-induced thrombocytopenia. Clin. Cardiol. *41*, 1521–1526. https://doi.org/10.1002/clc.23061.

Stone, O.J., Pankow, N., Liu, B., Sharma, V.P., Eddy, R.J., Wang, H., Putz, A.T., Teets, F.D., Kuhlman, B., Condeelis, J.S., and Hahn, K.M. (2019). Optogenetic control of cofilin and αTAT in living cells using Z-lock. Nat. Chem. Biol. *15*, 1183–1190. https://doi.org/10.1038/s41589-019-0405-4.

Stratton, M.M., and Loh, S.N. (2010). On the mechanism of protein fold-switching by a molecular sensor. Proteins *78*, 3260–3269.

Stratton, M.M., Mitrea, D.M., and Loh, S.N. (2008). A Ca^{2+}-sensing molecular switch based on alternate frame protein folding. ACS Chem. Biol. *3*, 723–732.

Sun, Y., Yu, L., Liu, C., Ye, S., Chen, W., Li, D., and Huang, W. (2021). One-tube SARS-CoV-2 detection platform based on RT-RPA and CRISPR/Cas12a. J. Transl. Med. *19*, 74. https://doi.org/10.1186/s12967-021-02741-5.

Suzuki, K., Kimura, T., Shinoda, H., Bai, G., Daniels, M.J., Arai, Y., Nakano, M., and Nagai, T. (2016). Five colour variants of bright luminescent protein for real-time multicolour bioimaging. Nat. Commun. *7*, 13718. https://doi.org/10.1038/ncomms13718.

Tochio, N., Umehara, T., Nakabayashi, K., Yoneyama, M., Tsuda, K., Shirouzu, M., Koshiba, S., Watanabe, S., Kigawa, T., Sasazuki, T., et al. (2015). Solution structures of the DNA-binding domains of immune-related zinc-finger protein ZFAT. J. Struct. Funct. Genomics *16*, 55–65. https://doi.org/10.1007/s10969-015-9196-3.

Verhoef, L.G.G.C., Mattioli, M., Ricci, F., Li, Y.-C., and Wade, M. (2016). Multiplex detection of protein–protein interactions using a next generation luciferase reporter. Biochim. Biophys. Acta *1863*, 284–292. https://doi.org/10.1016/j.bbamcr.2015.11.031.

Wang, R.E., Zhang, Y., Cai, J., Cai, W., and Gao, T. (2011). Aptamer-based fluorescent biosensors. Curr. Med. Chem. *18*, 4175–4184.

Whitesides, G.M., and Grzybowski, B. (2002). Self-assembly at all scales. Science *295*, 2418–2421. https://doi.org/10.1126/science.1070821.

Woods, D., Doty, D., Myhrvold, C., Hui, J., Zhou, F., Yin, P., and Winfree, E. (2019). Diverse and robust molecular algorithms using reprogrammable DNA self-assembly. Nature *567*, 366–372. https://doi.org/10.1038/s41586-019-1014-9.

Xu, X., Lemmens, L.J.M., den Hamer, A., Merkx, M., Ottmann, C., and Brunsveld, L. (2020). Modular bioengineered kinase sensors via scaffold protein-mediated split-luciferase complementation. Chem. Sci. *11*, 5532–5536. https://doi.org/10.1039/D0SC00074D.

Yin, P., Choi, H.M.T., Calvert, C.R., and Pierce, N.A. (2008). Programming biomolecular self-assembly pathways. Nature *451*, 318–322. https://doi.org/10.1038/nature06451.

Yurke, B., Turberfield, A.J., Mills, A.P., Simmel, F.C., and Neumann, J.L. (2000). A DNA-fuelled molecular machine made of DNA. Nature *406*, 605–608. https://doi.org/10.1038/35020524.

Zadeh, J.N., Steenberg, C.D., Bois, J.S., Wolfe, B.R., Pierce, M.B., Khan, A.R., Dirks, R.M., and Pierce, N.A. (2011). NUPACK: analysis and design of nucleic acid systems. J. Comput. Chem. *32*, 170–173. https://doi.org/10.1002/jcc.21596.

Zheng, H., Bi, J., Krendel, M., and Loh, S.N. (2014). Converting a binding protein into a biosensing conformational switch using protein fragment exchange. Biochemistry *53*, 5505–5514. https://doi.org/10.1021/bi500758u.

STAR★METHODS

KEY RESOURCES TABLE

REAGENT or RESOURCE	SOURCE	IDENTIFIER
Bacterial and virus strains		
E. Coli BL21 (DE3) cells	Novagen	69450
E. Coli TOPO cells	Invitrogen	C4040
Chemicals, peptides, and recombinant proteins		
Carbanecillin	Millipore Sigma	C1389
IPTG	GoldBio	12481C100
DNaseI	Sigma	DN25
Lysozyme	GoldBio	L-050-25
Imidazole	Alfa Aesar	A120221
DMSO	Corning	25950CQC
Furimazine	Aobious	AOB36539
T4 DNA ligase	Thermo Fisher	EL001
Phusion Polymerase	New England Biolabs	M0530L
Tris Base	Fisher Bioreagents	BP152
Borate	Sigma	B-0252
EDTA	Fisher Bioreagents	BP118
Tween-20	Fisher Biotech	9005-64-5
NaCl	EMD	BDH9286
Serotonin	Millipore Sigma	14927
ATP	Millipore Sigma	A26209
Urea	Fisher Chemical	57-13-6
Acrylamide	National Diagnostics	EC-849
Deposited data		
All raw and analyzed data	This paper	https://doi.org/10.17632/tfvsb7gz7n.1
Oligonucleotides		
DNA oligonucleotides used in this study, see Table S2	This paper	N/A
Recombinant DNA		
pET-25b(+)	Novagen	69753
pET-41a(+)	Novagen	70556
GeNL/pcDNA3	Addgene	85200
pET41-GeNL	This paper	N/A
pET25-nLucCP50	This paper	N/A
pET25-GeNL_GCN4 at pos 50	This paper	N/A
All pET25-nLuc-AFF Constructs	This paper	N/A
Software and algorithms		
Kaleidagraph	Synergy Software	Version4.5.2
ImageJ	Schneider et al. (2012) *Nature Methods* 9(7),671-675	imagej.nih.gov
Nupack	Zadeh et al. (2011) *J Comput Chem*, 35 :170-173	nupack.org
Other		
LB Medium	BD Biosciences	244610
FBS	Corning	35-010-CV
BSA	New England Biolabs	B9000S
Nickel-Nitrilotriacetic Agarose Resin	MCLAB	NINTA-300
Superose 6 Increase 10/300 GL	Cyvita	GE29-0915-956

(*Continued on next page*)

Continued

REAGENT or RESOURCE	SOURCE	IDENTIFIER
96-well assay plates	Costar	3789A
Spectramax i3x plate Reader	Molecular Devices	tinyurl.com/yckmm6zc
OnePlus 7 Pro	OnePlus	GM1917

RESOURCE AVAILABILITY

Lead contact

Further information and requests for resources and reagents should be directed to and fulfilled by the Lead Contact, Stewart N. Loh (lohs@upstate.edu).

Materials availability

Plasmids generated in this study will be shared without restriction by the lead author upon request, until made available publicly in Addgene.

Data and code availability

- All raw data and images generated in this paper have been deposited to Mendeley Data: Sekhon, Harsimranjit; Loh, Stewart (2022), "Engineering Protein Activity into Off-the-Shelf DNA Devices", Mendeley Data: https://doi.org/10.17632/tfvsb7gz7n.1. The DOI is also listed in the Key resources table.
- This paper does not report original code.
- Any additional information required to reanalyze the data reported in this paper is available from the lead contact upon request.

METHOD DETAILS

Gene construction and protein purification

All expression constructs here were cloned into pET25 vector, which contains a C-terminal 6x-His tag. The GeNL/pcDNA3 gene was a gift from Takeharu Nagai (Addgene plasmid # 85200; http://n2t.net/addgene:85200; RRID:Addgene_85200). The GeNL gene was inserted into the expression vector at the NdeI/XhoI sites along with a C-terminal 6xHis tag. Extension PCR was used to insert the GCN4 gene into the GeNL gene (at amino acid position 50 – 51 of the nLuc amino acid sequence) as well as to add KpnI and NheI restriction sites at the 5′- and the 3′-ends (respectively) of the resulting nLuc-AFF gene. Linker length variants of the nLuc-AFF gene were constructed by synthesizing primers with various linkers as well as a NotI restriction site and assembling the new gene via overlapping PCR. All genes were fully sequenced. Protein sequences are shown in Table S1.

Proteins were expressed in *E. coli* BL21(DE3) cells with isopropyl β-D-thiogalactopyranoside induction for 16 – 18 h at 18°C. Cell pellets were resuspended in 20 mM Tris (pH 7.5), 0.5 M NaCl, 15 mM imidazole, 0.1% Tween 20 and lysed with a small amount of lysozyme followed by sonication (4 × 20 s pulses on ice). Viscosity was reduced by adding $MgSO_4$ to final concentration of 5 mM along with DNase I, and the soluble fraction was loaded onto a nickel-nitrilotriacetic acid column (Bio-Rad) with purification following the manufacturer's protocol. Eluted proteins were dialyzed into 20 mM Tris (pH 8.5), 150 mM NaCl and further purified using a Superose 6 Increase 10/300GL size-exclusion column (Cytiva). For purity determination, proteins were run on 0.02% SDS polyacrylamide gels and imaged on a Sapphire Biomolecular Imager (Azure Biosystems) to detect fluorescence from the mNG domain, which remains native in these conditions. nLuc-AFF purity was judged to be ~70% by this method, with the remaining 30% consisting of C-terminally truncated products (Figure S3C).

Luminescence measurements and image processing

Luminescence was measured using a SpectraMax i3 plate reader (Molecular Devices) with the following settings: 150 μL samples, 1 mm read height, 400 – 600 nm scans with 5 nm intervals). Furimazine (Aobious, catalog #36569) was added to a final concentration of 50 μM, and this solution was aged for at least 10 min at room temperature prior to recording luminescence spectra. Biosensor performance was quantified by the ratio of luminescence intensity at 460 nm and 520 nm (L460/L520). Quantification of samples by luminescence spectra and cell phone camera was performed on the same samples in the same plate (Corning Costar 96-well assay plates, white polystyrene, round bottom).

Cell phone images were taken using a OnePlus 7 Pro with the following settings: ISO 200, f/1.6 and auto WB. For quantification, images were split into the blue and green channels using ImageJ (Schneider et al., 2012), and intensity in each channel was quantified by manually drawing a circle inside each well and calculating the average intensity. The average intensity in the blue channel was then divided by the average intensity in the green channel. To ensure that all the samples within the same experiment were imaged in the same field, any experiment that contains more than 6 samples (Figures 2C, 2D, 3F, and S5H) were split into two separate rows on the 96-well plate. The two rows were then imaged, and the final images were cropped and stitched for displaying. For all images

shown, contrast was adjusted for display only without any modification of the raw grayscale values for each channel. Raw images without any contrast adjustment or cropping can be found in the DOI listed in the key resource table.

Biosensor performance characterization

The performance of nLuc-AFF biosensor was characterized by the turn-on as well as the binding affinity of GCN4 to its consensus AP-1 sequence. We purified the nLuc-AFF three independent times (biological repeats) and performed three technical repeats of each biological repeat. To determine the switching efficiency, we mixed 30 nM of nLuc-AFF with either 2 μM of AP-1 containing double-stranded oligonucleotide (AGTGGAGATGACTCATCTCGTGC), 2 μM of the non-consensus double-stranded oligonucleotide (GTTCCAGGTTAAGAAGTGCTCTCAGGGTGGCGCGGC), or no oligonucleotide. Buffer was 20 mM Tris (pH 8.5), 150 mM NaCl, 0.1 mg/mL BSA. Samples were mixed and incubated overnight, in the dark, at room temperature, and scanned/photographed the next day. Equilibrium binding experiments were performed in triplicate by mixing 30 nM protein with various concentrations of AP-1 (2-fold serial dilutions starting from 2 μM) and incubating them overnight, in the dark, at room temperature. Buffer was 20 mM Tris (pH 8.5), 150 mM NaCl, and either 0.1 mg/mL BSA or 10% FBS. Cell phone images and luminescence spectra were recorded for all samples, and the signals were fit to the one-site quadratic binding equation to obtain K_D.

For experiments in serum, 2 M Tris (pH 8.5) was added to freshly thawed fetal bovine serum to a final concentration of 20 mM. This solution was then diluted to the desired serum concentration in 20 mM Tris (pH 8.5), 150 mM NaCl. The DNA and protein concentrations were identical to those described above. For integrated intensity measurements, biosensor was diluted in either 25%, 50%, 75%, or 100% serum to a final concentration of 30 nM, and total luminescence was calculated by integrating the spectra from 400 – 600 nm.

Oligonucleotide design and purification

Oligonucleotides were designed using NUPACK to ensure metastability as well as high efficiency of TMSD. The two sequences of the nCoV genome used in this study were chosen from the CDC RT-PCR Diagnostic Panel: sequence N1 (cagattcaactggcagtaaccaga) and sequence N2 (tcagcgttcttcggaatgtcgcgc). The serotonin and ATP aptamers were also designed using NUPACK. Synthetic oligonucleotides were ordered from Eurofins Genomics without purification and were purified in-house (see Table S2 for oligonucleotide sequences).

Oligonucleotides were purified using urea PAGE (7 M urea, 8% acrylamide:bis 19:1, 1x Tris-borate-EDTA [TBE]). Samples (100 μL of 50 μM oligonucleotide in 50% formamide, 0.01% bromophenol blue) were loaded on a 55°C prewarmed 16.5 × 19 cm gel and run at 200 V for 2 h with heating by a circulating 55°C water bath. Gels were stained in 2% methylene blue for 20 m and briefly rinsed with water. Bands were excised, crushed, and mixed with ~5 volumes elution buffer (20 mM Tris pH 7.5, 0.5 M NaCl, 1 mM EDTA). After 2 freeze-thaw cycles at −80°C, the tubes were shaken overnight at 37°C. The samples were then centrifuged to remove gel fragments, and an equivalent volume of 1-butanol was added with vigorous vortexing. The organic phase was discarded, and 1/5 volume of 3 M sodium acetate (pH 5.2) was added along with 2.5x volume of 95% ethanol pre-chilled at −80°C. These samples were kept at −80°C for 1 h then centrifuged at 16,000 x *g* for 30 m at 4°C. The supernatant was discarded and the pellet was rinsed with chilled 95% ethanol, centrifuged at 16,000 x *g* for 30 min at 4°C, and dried at 37°C for 20 min. The pellet was suspended in ddH_2O and concentration was determined by nanodrop.

Toehold mediated strand displacement and logic gate experiments

Hairpins were snap-cooled separately in 20 mM Tris (pH 8.5), 150 mM NaCl at a concentration of 3 μM, by heating to 95°C for 3 min and rapidly cooling to room temperature using a thermal cycler. For validation by PAGE, 500 nM of probes were mixed with 500 nM of triggering oligonucleotide in 20 mM Tris (pH 8.5), 150 mM NaCl and incubated at room temperature for 3 h. Samples were then loaded on 12% acrylamide:bisacrylamide (19:1) gel in 1x TBE buffer and run in TBE for 40 min at room temperature. Gels were then stained with ethidium bromide and imaged. For logic gate experiments, hairpins and nLuc-AFF were mixed to a final concentration of 300 nM and 30 nM, respectively, in 20 mM Tris (pH 8.5), 150 mM NaCl, 0.1 mg/mL BSA. Triggering oligonucleotides were then added to a final concentration of 600 nM and the reaction was allowed to proceed overnight at room temperature before luminescence was recorded.

Validation of nLuc-AFF with DNA aptamers

Serotonin and ATP aptamers were purified and snap-cooled before use as described above. For PAGE assays, 250 nM of aptamer was mixed with 500 nM of naked AP-1 in 20 mM Tris (pH 8.5), 0.15 mM NaCl, whereupon either 10 μM serotonin, 2 mM ATP, or DMSO vehicle (final concentration 0.05%) was added, and the reaction was allowed to proceed for 2 h at room temperature. Samples were then loaded on a 12% polyacrylamide gel and run in TBE buffer. Gels were stained with ethidium bromide and imaged. For luminescence assays, 250 nM aptamer, and 250 nM naked AP-1, and 30 nM nLuc-AFF were mixed, and either 10 μM serotonin or 2 mM ATP was added. Samples were kept overnight at room temperature before recording luminescence spectra the next day. Buffer was 20 mM Tris (pH 8.5), 150 mM NaCl, 0.1 mg/mL BSA, 5 mM $MgCl_2$.

Serotonin aptamer equilibrium binding

Serotonin aptamer and the corresponding naked AP-1 oligonucleotide were individually snap-cooled as described above and mixed with 50 nM nLuc-AFF at a final concentration of 250 nM each in 20 mM Tris (pH 8.5), 150 mM NaCl, 0.1 mg/mL BSA, 5 mM $MgCl_2$.

Serotonin concentrations were prepared by 2-fold serial dilution starting 40 μM. Samples were maintained at room temperature overnight. Luminescence was quantified by both L460/L520 ratio and cell phone image and data were fit to the one-site binding equation to obtain K_D.

Biosensor turn-on kinetics

Freshly thawed biosensor (100 nM) was either mixed with 1 μM AP1 oligonucleotide or the same volume of buffer in 20mM Tris (pH 8.5), 150 mM NaCl, 0.1 mg/mL BSA. At the indicated timepoints, 150 μL of the mix was transferred to a fresh tube, furimazine added to final concentration of 50 μM, and spectra recorded as described above. The luminescence change was fit to a single exponential function to obtain the half time. For samples photographed by cell phone, 1 μM AP-1 oligonucleotide was added to a solution of 100 nM nLuc-AFF in 20 mM Tris (pH 8.5), 150 mM NaCl, 0.1 mg/ml BSA in separate tubes separated in time by 15 min 60 min after mixing the first sample, furimazine was added to a final concentration of 50 μM, and the reactions were aged for 10 min before imaging.

Determination of the limit of detection

LoD of AP-1 via TMSD was determined by mixing 100 nM of each of the two snap-cooled probes with 30 nM of nLuc-AFF in 20 mM Tris (pH 8.5), 150 mM NaCl, 0.1 mg/mL BSA. SARS2 sequence was then added at various concentrations in triplicate, starting at 140 nM and performing serial 1.8-fold dilutions to a final concentration of 0.4 nM. Tubes were kept overnight at room temperature and luminescence was recorded after adding furimazine to a final concentration of 50 μM. LoD for cell phone images and luminescence spectra were then determined by selecting the range of AP-1 that produced a linear change in luminescence and fitting to a linear equation. For each of the three replicates, we calculated LoD using the following equation: LoD = 3.3δ/slope(Lavín et al., 2018), where δ is the standard deviation of the y-intercept. These results were verified by determining the AP-1 concentration at which the signal was >3 s.d. away from the signal of the sample with no AP-1 added. This procedure was repeated with two biological repeats, each with 3 technical repeats.

AP-1 binding by fluorescence anisotropy

For equilibrium binding experiments, 30 nM of nLuc-AFF was mixed with various concentrations of AP-1 (2-fold serial dilutions starting from 2 μM) in 20 mM Tris (pH 8.5), 150 mM NaCl, 0.1 mg/mL BSA. This mixture was kept at room temperature in the dark overnight, and fluorescence anisotropy was then recorded the next day in a 96-well plate (Costar, black polystyrene, round bottom) using Molecular Instruments i3x plate reader with the following settings: 100 μL total volume, 1.1 mm read height, 500 ms integration time. The experiment was repeated in triplicate and the signals were fit to the one-site quadratic binding equation to obtain K_D.

To determine the rate of AP-1 binding by anisotropy, freshly thawed nLuc-AFF was diluted to 30 nM in triplicate and either 2 μM AP-1 or NC oligo was added to each of the three replicates in 20 mM Tris (pH 8.5), 150 mM NaCl, 0.1 mg/mL BSA. No DNA was added to the control samples. Anisotropy values were recorded at various time points with the samples kept in the dark at room temperature between readings. Data were fit into a single exponential function to obtain the turn-on rate.

QUANTIFICATION AND STATISTICAL ANALYSIS

Biosensor signal for each experiment is expressed as mean ± SD of 3 independent repeats. Data analysis was performed using Kaleidagraph. Significance was determined using an unpaired t-test in Kaleidagraph, and differences were considered statistically significant at $p < 0.05$. Statistical details for every individual experiment can be found in the results and figure legends.